Warm Electron-Driven Whistler Instability in an Electron-Cyclotron–Resonance Heated, Mirror-Confined Plasma

R. C. Garner,[a] M. E. Mauel,[b] S. A. Hokin, R. S. Post, and D. L. Smatlak

Plasma Fusion Center, Massachusetts Institute of Technology, Cambridge, Massachusetts 02139

(Received 8 May 1986; revised manuscript received 24 February 1987)

The whistler electron microinstability has been observed in the Constance-*B* quadrupole-mirror, electron-cyclotron–resonance heated plasma. Experimental evidence indicates that the warm-electron component (2 keV) drives the instability while the hot-electron component (400 keV) is stable. Dispersion-relation calculations using a new distribution function (electron-cyclotron–resonance heated distribution) to model the warm-electron component are in agreement with this experimental result.

PACS numbers 52.35.Qz, 52.35.Hr, 52.55.Jd

The whistler instability is an electron microinstability which may be present in a plasma with an anisotropic electron velocity-space distribution. Mirror-confined plasmas in which the electrons are heated by electron-cyclotron–resonance heating (ECRH) have anisotropic electron distributions.[1] Past experiments of this type have demonstrated the existence of the whistler instability.[2-5] In these experiments rf emission in the electron-cyclotron range of frequencies is observed and is typically accompanied by enhanced particle end loss induced by the unstable waves. While the frequency spectrum and power of the rf emission has been measured in many cases, it has been difficult to determine which regions of velocity space drive microinstability. We show that the plasma of the Constance-*B* mirror experiment is microunstable. We identify this instability as the whistler and present experimental evidence which shows that it is driven by the warm-electron component (2 keV), while the hot-electron component (400 keV) is stable. The identification of this instability is based upon good agreement between the observed frequency of emission and the prediction of the most unstable frequency obtained from dispersion-relation calculations. For these calculations, the warm electrons are modeled with a new distribution function (ECRH distribution) which more accurately describes the electron velocity-space response to ECRH. In addition, our instability analysis identifies which regions of velocity space drive the instability.

Constance-*B* is a quadrupole magnetic mirror experiment in which a hydrogen plasma is produced and heated by 1 kW of rf at 10.5 GHz. The nonrelativistic cyclotron frequency on axis at the midplane is 8.4 GHz. Three distinct electron-energy components are detected. Electrostatic gridded end-loss analyzers detect a 150 eV, electrostatically confined cold-electron component and a 2-keV warm-electron component (see Fig. 1). Si(Li), germanium, and NaI x-ray detectors, which measure bremsstrahlung photons with energies greater than 1 keV, identify a hot-electron component which is heated at 450 keV/s until a 400 keV steady-state temperature is attained. An interferometer indicates that the hot component contributes approximately half of the total line density of 3.5×10^{12} cm^{-2}. The midplane plasma diameter is 20 cm. X-ray measurements do not detect the warm-electron component which indicates that the warm-electron density is less than 0.1 of the hot-electron density.

The rf emission associated with the microinstability occurs in fairly regular bursts (period $\simeq 1$ ms, energy per burst $\simeq 5\times10^{-6}$ J, burst time $\simeq 5$ μs) with frequencies in the range 6.7–8.7 GHz. These rf emission bursts correlate with electron end-loss bursts (see Fig. 2) as well as bursts of ion end loss and diamagnetism, and potential fluctuations.

The following evidence shows that the microinstability is driven by the warm-electron component while the hot-electron component is stable and has little effect on microinstability.

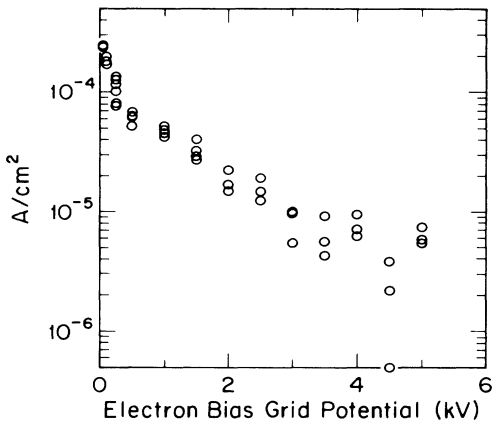

FIG. 1. Energy distribution of the electron end loss observed with the electrostatic gridded end-loss analyzers. Two different average energies are observed. Each point corresponds to the average current (mapped to the midplane) over a 40-ms time window at identical times during different shots. The warm-component end-loss current consists of bursts due to microinstability and an average level which exists both during and between bursts.

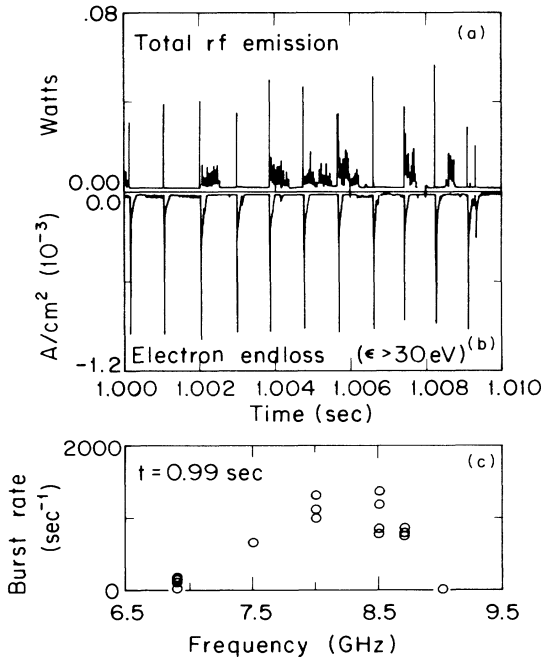

FIG. 2. (a) Bursts of rf emission with frequencies in the range 5.25 to 12 GHz. (b) Bursts of electron end loss. (c) Frequency spectrum of the rf emission (each point corresponds to $\delta f = 1$ MHz).

(1) There is no unstable rf emission from a plasma which contains just a hot-electron component. Such a plasma can be produced by turning off the gas source during the shot while leaving the ECRH on as shown in Fig. 3, or by turning off the ECRH. In the latter case the unstable rf emission bursts sporadically for several milliseconds and then completely stops. The end-loss analyzers indicate that the electrons with energies less than 5 keV, which are responsible for more than 99% of the total electron end-loss current, leave within approximately 5 ms after ECRH is turned off. The x-ray detector indicates that the hot-electron temperature increases after ECRH is turned off and the diamagnetic loop together with the x-ray detector indicates that hot-electron density decays exponentially with a 1-s time constant (see Fig. 4).

(2) The unstable emission begins less than 1 ms after the gas breaks down, before a hot component exists. The average emission power becomes constant in time approximately 1 to 5 ms after it begins. The temperature determined from the x-ray spectrum is only 10 keV 20 ms after the gas breaks down (the earliest total spectrum measured).

(3) The average unstable rf emission power (averaged over many bursts) is constant in time during ECRH, whereas the hot-electron temperature varies in time (see Fig. 4).

Although the hot-electron component does not drive

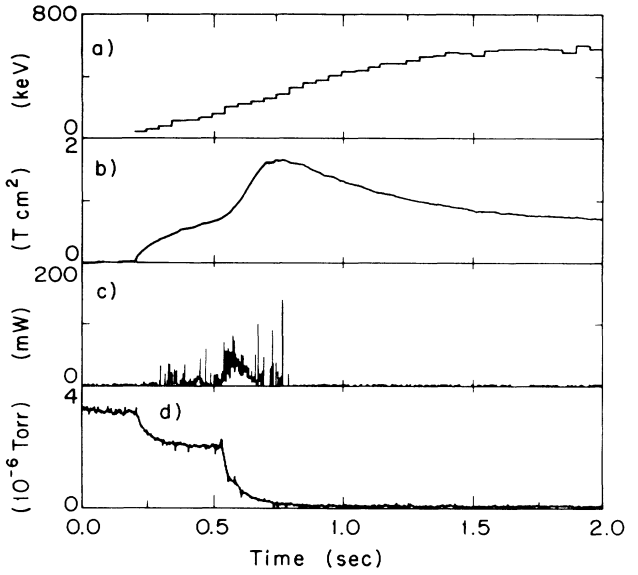

FIG. 3. Data showing the stability of the hot component. The gas is turned off at 0.6 s while the ECRH is left on until 2 s. The hot component has the longest confinement and remains for several seconds after the cold and warm components have decayed. There is no unstable rf emission during this time. (a) Hot-electron temperature. (b) Diamagnetic flux. (c) Power of total unstable rf emission. Data-taking method for this figure does not reveal individual rf emission bursts. (d) Gauge pressure.

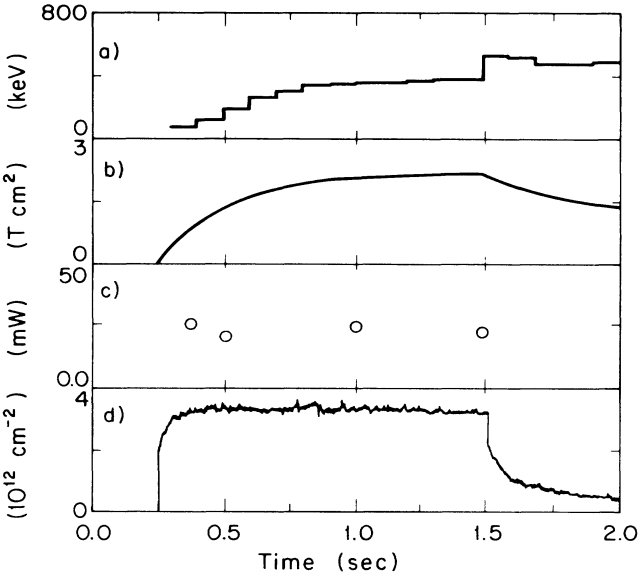

FIG. 4. (a) The temperature of hot electrons determined by unfolding the x-ray spectrum with a Maxwellian distribution, every 100 ms. Average over several shots. (b) Diamagnetic flux. (c) Power of the unstable rf emission. Each point corresponds to the average emission power at the detector in a 40-ms time window. (d) Line density.

the whistler instability there is still hot-electron end loss induced by the instability when a warm-electron component is present. The total power loss due to instability-induced end loss is approximately 90 W for the warm electrons and 80 W for the hot electrons when the ECRH power is 1 kW. Approximately 1% of the total electron end-loss current consists of hot-electron end loss with an average energy of 400 keV. A scintillator probe, sensitive to electrons with $\langle E\rangle \simeq 100$ keV, indicates that (30–50)% of this hot-electron end loss is caused by interactions with the unstable waves (the remainder is caused by interactions with the ECRH waves). Since the hot electrons do not drive microinstability as was shown above, this implies that hot electrons may gain energy from the unstable waves as well. However, there is a net energy loss because the hot electrons which diffuse downward in energy due to the unstable waves have a chance to enter the loss cone and carry their total energy out of the plasma.

Dispersion relation calculations which use a new distribution function, the ECRH distribution, to model the warm-electron component identify the instability as the whistler instability. Other distributions which have also been used in the past (e.g., bi-Maxwellian and loss-cone distributions) predict unstable whistler wave frequencies which are approximately 20% lower than the experimentally measured frequencies of the unstable waves of Constance-B.[6] The ECRH distribution is

$$f_0(E,\mu)=\exp\left[-\frac{\chi}{T_\chi}-\theta(\eta)\frac{\eta}{T_{\eta+}}+\theta(-\eta)\frac{\eta}{T_{\eta-}}\right], \tag{1}$$

where $\chi=\frac{1}{2}(E+\mu B_h)$, $\eta=\frac{1}{2}(E-\mu B_h)$, $E=mc^2(\gamma-1)$ is the particle kinetic energy, $\mu=\frac{1}{2}mu^2/B$ is the magnetic moment, $u/c=(\gamma^2-1)^{1/2}$ is the relativistic velocity, $\theta(\eta)$ is the unit step function, $B_h=\omega_h m_0 c/e$, and ω_h is the applied ECRH frequency. The lines defined by $\eta=$const are the diffusion paths for electrons which interact with waves of frequency ω_h. Contours of f_0 in relativistic velocity space are plotted in Fig. 5(a). They closely resemble the contours of distribution functions which are numerically generated by Fokker-Planck simulations of ECRH, mirror confined plasmas.[1] Unlike distributions used in the past, Eq. (1) more accurately reflects the electron velocity-space response to the heating waves. It does not allow for unstable waves with frequency above the ECRH frequency, which agrees with experiment. The region defined by $\eta>0$ is destabilizing for a wave and the region defined by $\eta<0$ is stabilizing for a wave. The boundary between these regions follows the discontinuity in the derivative of f_0. For the nonrelativistic case the boundary is defined by the line $u_\parallel/c=u_\perp/c$.

Local dispersion-relation calculations were done for a range of locations along the axial magnetic-field line and

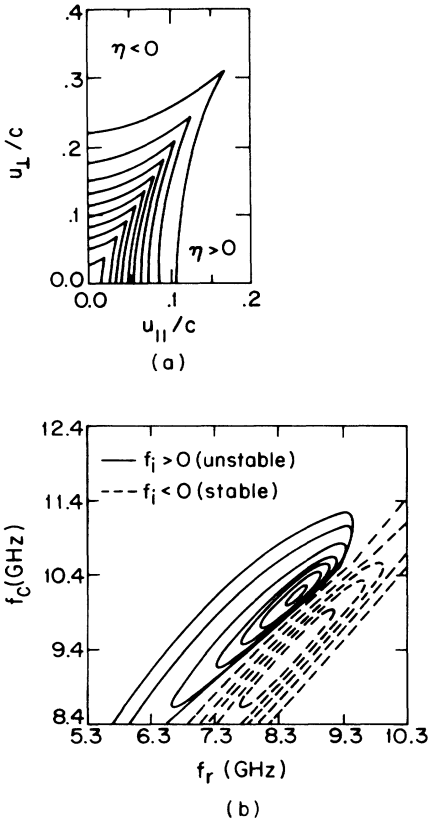

FIG. 5. (a) Contours of Eq. (1) in relativistic velocity space for $T_\chi=5$ keV, $T_{\eta+}=0.5$ keV, and $T_{\eta-}=0.25$ keV. These values give $\langle E\rangle=\frac{1}{2}m_e\int v^2 f_0=5$ keV. Experimental values of T_χ and T_η are not known. These values were chosen to provide a representative example of a dispersion-relation calculation for an unstable warm plasma. The behavior of the contours of the growth rate determined by these calculations is not sensitive to changes in these temperature parameters as long as $T_\chi/T_{\eta\pm}>1$ and the absolute values of each parameter are below certain thresholds dependent on this ratio. (b) Contours of f_i with the temperature parameters above. The vertical axis is the local cyclotron frequency and corresponds to the position along a field line. The horizontal axis is the real frequency of a wave that satisfies the cold-plasma dispersion relation with $k_\perp=0$. The twelve contour levels shown are, relative to the maximum, -0.9 to 0.9 in steps of 0.2 and the contour levels 0.01 and 0.001. The frequency corresponding to the maximum growth rate is only sensitive to changes in the ECRH frequency. This is consistent with experimental observations.

for a range of wave frequencies. In these calculations the growth rate ω_i was determined in the following manner[7]:

$$\omega_i=\frac{\mathbf{E}^*\cdot\mathbf{D}^a\cdot\mathbf{E}}{\mathbf{E}^*\cdot(\partial\mathbf{D}^h/\partial\omega_r)\cdot\mathbf{E}}, \tag{2}$$

where $\mathbf{E}$ is the electric-field amplitude, $\mathbf{D}^a$ is the anti-Hermitean part of the relativistic Vlasov dispersion tensor, and $\mathbf{D}^h$ is the cold, fluid dispersion tensor (which

is Hermitean). Figure 5(b) shows the contours of $f_i = \omega_i/2\pi$ for a particular choice of the temperature parameters. The vertical axis gives the local relativistic cyclotron frequency, with 8.4 GHz the midplane cyclotron frequency. The horizontal axis gives the wave frequency. For this calculation $k_\perp$ is set to zero (whistler waves) because previous calculations have shown the growth rates to be greatest for $k_\perp = 0$. The most unstable wave frequencies predicted by this calculation match the frequencies of the unstable whistler waves observed in the experiment [see Fig. 2(c)]. An interesting feature of the ECRH distribution is that if the average energy is greater than some threshold ($\langle E \rangle = 40$ keV for $T_\chi | T_{\eta+} | T_{\eta-} = 36 | 3.6 | 1.8$ keV) then calculations performed with the relativistic form of $\mathbf{D}^a$ predict stable whistler waves. Calculations performed with the nonrelativistic form of $\mathbf{D}^a$ indicate no such threshold.[6] This is one possible explanation for the experimentally observed stability of the hot-electron component.

In summary, the whistler electron microinstability has been observed in the Constance-*B* quadrupole mirror, ECRH plasma. Experimental evidence indicates that the warm electrons drive the instability while the hot electrons are stable. Dispersion relation calculations using the ECRH distribution function, which describes the response of warm electrons to ECRH, predict unstable whistler wave frequencies which match the experimentally measured unstable frequencies. These calculations also suggest that relativistic effects are stabilizing.

This work was supported by the U.S. Department of Energy, under Contract No. DE-AC02-78ET51013.

---

[a]Present address: PhotoMetrics, Inc., 4 Arrow Drive, Woburn, MA 01801.

[b]Present address: Department of Applied Physics, Columbia University, New York, NY 10027.

[1]M. E. Mauel, Phys. Fluids **27**, 2899 (1984).

[2]R. A. Blanken and N. H. Lazar, Phys. Fluids **13**, 2752 (1970).

[3]H. Ikegami, H. Ikezi, M. Hosokawa, K. Takayama, and S. Tanaka, Phys. Fluids **11**, 1061 (1968).

[4]R. A. James, R. F. Ellis, and C. J. Lasnier, Bull. Am. Phys. Soc. **29**, 1187 (1984).

[5]J. H. Booske, W. D. Getty, and R. M. Gilgenbach, Phys. Fluids **28**, 3116 (1985).

[6]R. C. Garner, Ph.D. thesis, Massachusetts Institute of Technology, 1986 (unpublished).

[7]A. Bers, in *Basic Plasma Physics I*, edited by A. A. Galeev and R. N. Sudan (North-Holland, Amsterdam, 1983).